Characteristics of sea ice in the Okhotsk coastal polynyas revealed by satellites, ice-profiling sonar and digital camera observations

Sohey NIHASHI,[1,2] Naoto EBUCHI,[1] Yasushi FUKAMACHI,[1] Shuhei TAKAHASHI[3]

[1]*Institute of Low Temperature Science, Hokkaido University, Sapporo 060-0819, Japan*
[2]*Department of Mechanical Engineering, Tomakomai National College of Technology, 443 Nishikioka, Tomakomai, Hokkaido 059-1275, Japan*
E-mail: sohey@me.tomakomai-ct.ac.jp
[3]*Snow and Ice Research Laboratory, Kitami Institute of Technology, 165 Koen-cho, Kitami 090-8507, Japan*

ABSTRACT. The characteristics of ice in the Okhotsk coastal polynyas are examined. A map of AMSR-E thin-ice thickness in the northwest shelf region shows that most of the coastal polynya area is covered by thin ice with a thickness of 0.1 m. The thickness increases sharply at the edge of the polynya. From comparisons with QuikSCAT backscatter, the thin-ice area corresponds well with the low-backscatter area during almost all the coastal polynya period. A comparison with ice thickness measured by an ice-profiling sonar in the coastal polynya region of northeastern Sakhalin shows a similar relationship, with the backscatter tending to be low when the ice is thin. The averaged backscatter of thin ($\leq$0.1 m) ice is –19.6 $\pm$ 2.8 dB (horizontal polarization). The backscatter of thin ice is considered to be mainly determined by the surface roughness because volume scattering of thin ice is low due to the dielectric properties associated with the high salinity. The results of this study suggest that the coastal polynya is covered with grease ice/nilas whose surface is almost mirror smooth. This is confirmed by a comparison with photographs taken at the coastal polynya region near Magadan, Russia. At the outer edge of the coastal polynya, a region of relatively high backscatter (>–16 dB) exists, probably because it has a rougher ice surface than the polynya area. This suggests that ice motion in this area may be convergent.

1. INTRODUCTION

The Sea of Okhotsk (Fig. 1) is the southernmost sea in the Northern Hemisphere that has a sizeable seasonal ice cover. The initial freezing occurs at the northwest shelf (NWS) region from November. The ice cover reaches a maximum extent ($\sim 1.0 \times 10^6$ km^2 on average) from the end of February to the beginning of March, when ~50–90% of the sea is covered with ice. Sea ice can reach the coast of Hokkaido at around 44° N (e.g. Fig. 2a). The ice melts away by June.

In the northern part of the Sea of Okhotsk, coastal polynyas are formed by divergent ice drift due to prevailing cold offshore winds from Siberia, Russia (Martin and others, 1998; Nihashi and others, 2009). Most of the polynya area is covered with thin ice. Since the heat insulation effect of sea ice is greatly reduced in the thin-ice area, turbulent heat flux to the atmosphere at the coastal polynya surface is possibly two orders of magnitude larger than in the surrounding thicker-ice area (Maykut, 1978). This leads to very high ice production there.

In the Sea of Okhotsk, the NWS polynya is the highest-ice-production area (Fig. 1). Nihashi and others (2009) estimated cumulative ice production in a unit area during winter is ~11 m, from a heat-budget analysis using thin-ice thickness derived from the Advanced Microwave Scanning Radiometer for the Earth Observing System (AMSR-E). In the Antarctic Ocean, the highest-ice-production area is the Ross Sea polynya where annual cumulative ice production was estimated to be ~20 m (Tamura and others, 2008) by a similar method to that of Nihashi and others (2009). Although the winter period in the Sea of Okhotsk is about half that of the Antarctic Ocean, the ice production per unit time in the NWS polynya is comparable to that in the Ross Sea polynya.

In the NWS polynya, dense shelf water (DSW) is formed due to the large amount of brine rejection associated with high ice production (Shcherbina and others, 2003). The DSW is the densest water formed at the surface of both the Sea of Okhotsk and the North Pacific (Kitani, 1973) and is thought to be the main source of ventilation of the North Pacific Intermediate Water (Talley, 1991; Warner and others, 1996). The DSW modified in the Sea of Okhotsk passes through the Kuril Islands and spreads into the intermediate layer of the North Pacific (Martin and others, 1998; Shcherbina and others, 2003). Thus, in the North Pacific, the Sea of Okhotsk is the only area where the surface water exposed to the atmosphere can be carried to the intermediate layer (at depths of 200–800 m), and the DSW drives the overturning in the North Pacific. Nakanowatari and others (2007) suggested that, during the past 50 years, warming of the intermediate water and weakening of the overturning has occurred in the northwestern North Pacific, originating from the Sea of Okhotsk.

Coastal polynyas play an important role in the climate system through high ice production and DSW formation in both the Northern and Southern Hemispheres. However, in situ monitoring of coastal polynyas has been limited because of the severe weather and oceanic conditions in winter and the lack of a stable platform, unlike landfast and thick pack ice. Therefore, the characteristics of ice in coastal polynyas (e.g. distribution of thin-ice thickness and type) have not been well understood.

Ku-band backscatter data from the NASA scatterometer (NSCAT) and SeaWinds scatterometer on the Quick Scatterometer (QuikSCAT) satellite have been used to detect the multi-year ice and first-year ice areas (e.g. Long and Drinkwater, 1999; Kwok, 2004, 2007; Nghiem and others, 2006, 2007). Tonboe and Toudal (2005) classified the new (pancake) ice area in the Greenland Sea from the combination of active (QuikSCAT) and passive (Special Sensor Microwave/Imager (SSM/I)) microwave satellite data.

https://doi.org/10.3189/172756411795931624 Published online by Cambridge University Press

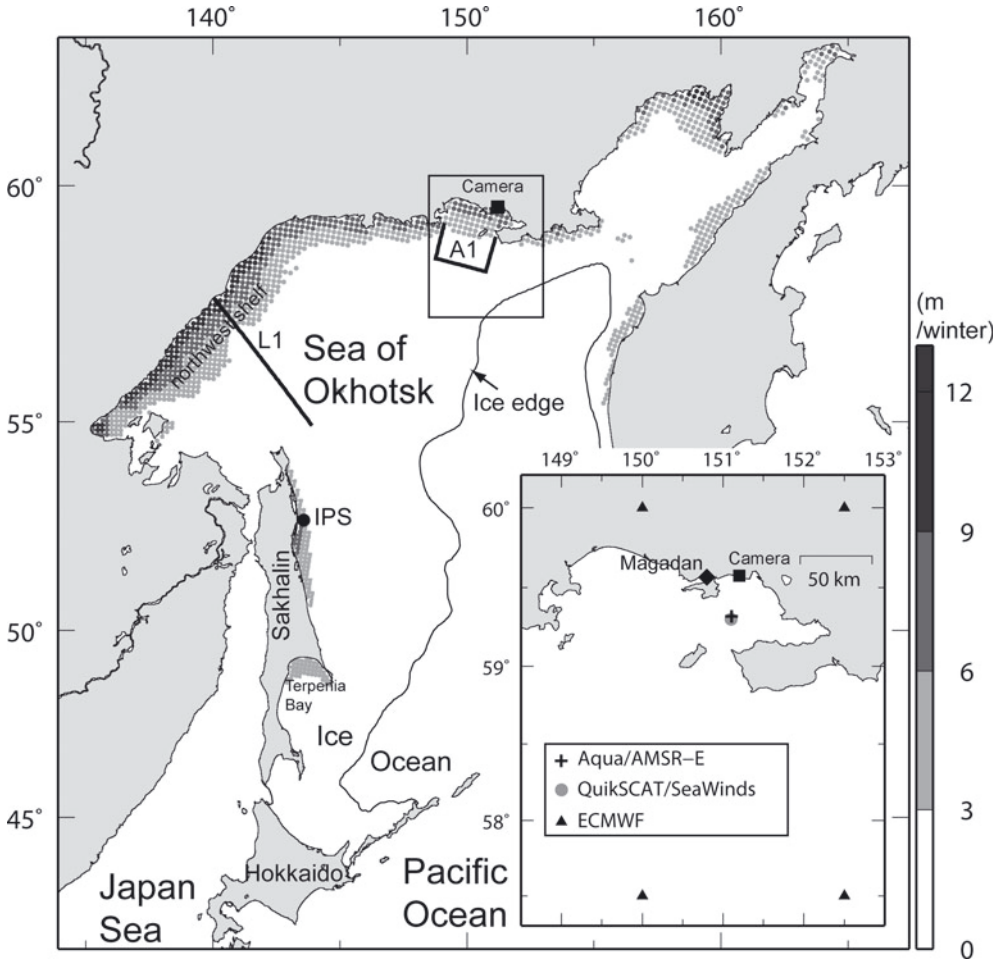

Fig. 1. Map of the Sea of Okhotsk showing the spatial distribution of cumulative sea-ice production during winter (December–March), averaged from the 2002/03–2004/05 seasons (after Nihashi and others, 2009). Thin black lines denote the mean February ice extent averaged from 2003 to 2005. The thick line, L1, is the analysis line. The area, A1, enclosed by a thick line is the analysis area. The locations of the ice-profiling sonar (IPS) and camera observations are shown by the black dot and square, respectively. The inset shows a map of the Magadan area where the camera observations were made. The cross (gray dot) indicates a gridpoint of AMSR-E (QuikSCAT) closest to the camera observation site. The four triangles indicate European Centre for Medium-Range Weather Forecasts (ECMWF) gridpoints close to the camera observation site.

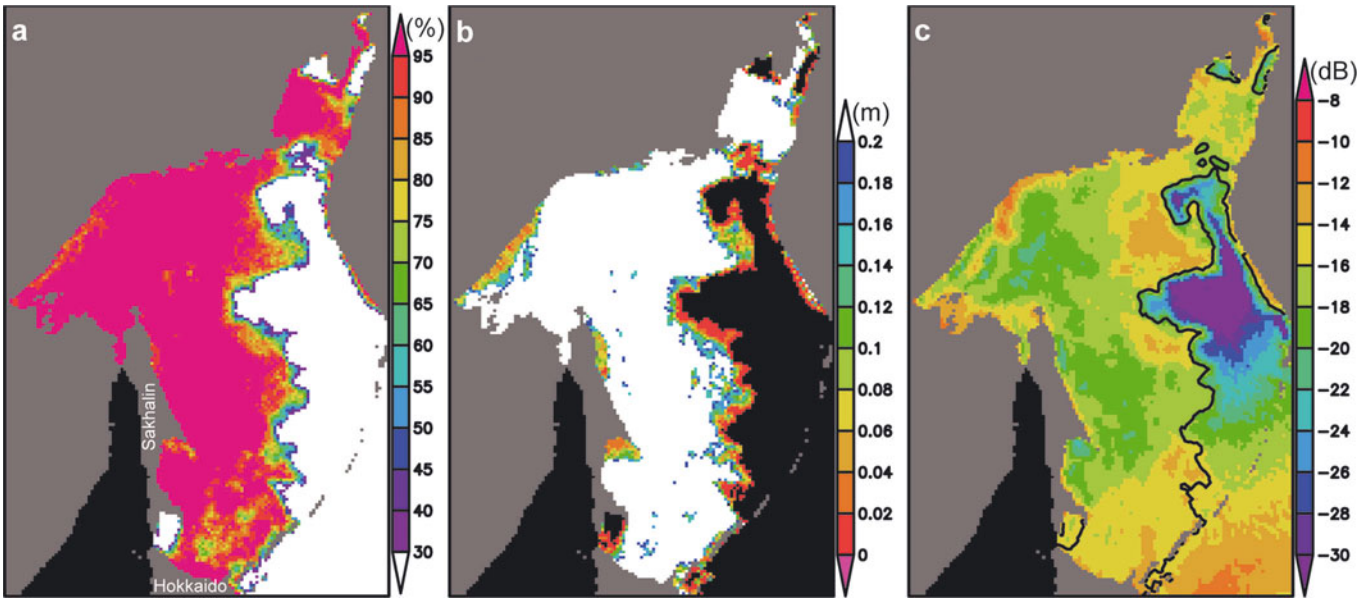

Fig. 2. Maps on 8 March 2003. The Japan Sea is masked by black. (a) Ice concentration derived from AMSR-E. (b) Thin-ice thickness derived from AMSR-E. The open ocean areas (ice concentration <30%) are masked black. (c) Horizontally polarized backscatter, σ^0, measured at incidence angle of 46° from QuikSCAT. Black lines denote ice edge.

https://doi.org/10.3189/172756411795931624 Published online by Cambridge University Press

In this study, the characteristics of sea ice in the Okhotsk coastal polynyas are examined using a comparison between the backscatter from QuikSCAT and thin-ice thickness from AMSR-E. The results from the satellite data analyses are validated using in situ data which included continuously measured ice draft in the coastal polynya region of north-eastern Sakhalin and daily photographs of the coastal polynya region taken from land near Magadan, Russia.

2. DATA

Normalized radar cross section (σ^0 or backscatter) from the QuikSCAT (Brigham Young University (UT, USA) daily browse images of QuikSCAT σ^0 measurements; Long, 2000) was used to detect ice type in the coastal polynyas. QuikSCAT operates at a frequency of 13.4 GHz (Ku band). The vertically and horizontally polarized backscatters are measured at incidence angles of 54° and 46° respectively, with daily temporal and 0.2° spatial resolutions.

Daily thin-ice thickness derived from AMSR-E was used for comparison with the QuikSCAT data. The ice thickness is estimated from the polarization ratio of the brightness temperature from the AMSR-E 36.5 GHz channels using an algorithm proposed by Nihashi and others (2009). The algorithm can estimate ice thickness of ≤0.2 m with accuracy of ±0.05 m. Ice concentration was also calculated using the enhanced NASA Team (NT2) algorithm (Markus and Cavalieri, 2000). The spatial resolution of the AMSR-E sea-ice data is ~12.5 km. All these satellite datasets were used for the December–March period during 2002/03–2006/07.

For comparison with the QuikSCAT data, ice draft measured by an ice-profiling sonar (IPS; ASL Environmental Sciences IPS4 420 kHz) in the coastal region of northeastern Sakhalin (52°43′ N, 143°34′ E; black dot in Fig. 1) was used. The IPS was moored from 27 December 2002 to 13 June 2003 at ~24 m depth. The sampling interval was 1 s and values are typically accurate to within ±0.05 m. The detail is described by Fukamachi and others (2009).

For validation of the results from the satellite data analyses, photographs were taken automatically by a digital camera (KONA SYSTEM Co., Ltd., now North One Co., LTD, KADEC-EYE) at 0900 h local time from the coast near Magadan, Russia (box in Fig. 1). This is a highly productive area for ice (Fig. 1), suggesting that the coastal polynya is well developed here. The camera was installed on a hill facing the sea, at ~50 m a.s.l., from September 2006 to September 2007. The image resolution of 336 × 288 pixels is enough to identify the sea-ice conditions.

For air temperature at 2 m, and surface sea-level pressure (SLP), we used the twice-daily (0000 and 1200 UT) data from the European Centre for Medium-Range Weather Forecasts (ECMWF) with a spatial resolution of 2.5° × 2.5°. The SLP was used to calculate the geostrophic wind. Hourly surface air temperature observed at the camera site near Magadan (box in Fig. 1) was also used.

3. RESULTS

3.1. Comparison between QuikSCAT backscatter and AMSR-E thin-ice thickness

Maps of AMSR-E ice concentration, AMSR-E thin-ice thickness and QuikSCAT backscatter (horizontal polarization) on 8 March 2003 are shown in Figure 2a–c. For the comparison, the backscatter is interpolated onto the AMSR-E grid with a Gaussian weighting function, with the e-folding scale and the influence radius set at 11.5 km and 23 km, respectively. The sea ice covers the Sea of Okhotsk extensively (Fig. 2a). Thin-ice areas corresponding to coastal polynyas are clearly identified in the NWS region, a coastal region of northeastern Sakhalin and Terpenia Bay (Fig. 2b). The backscatter tends to be high in the marginal ice zone, and low in the coastal polynya areas (Fig. 2c). The vertically polarized backscatter shows similar results (not shown here). Hereafter, we mainly use the horizontally polarized backscatter. The data on other days show similar results.

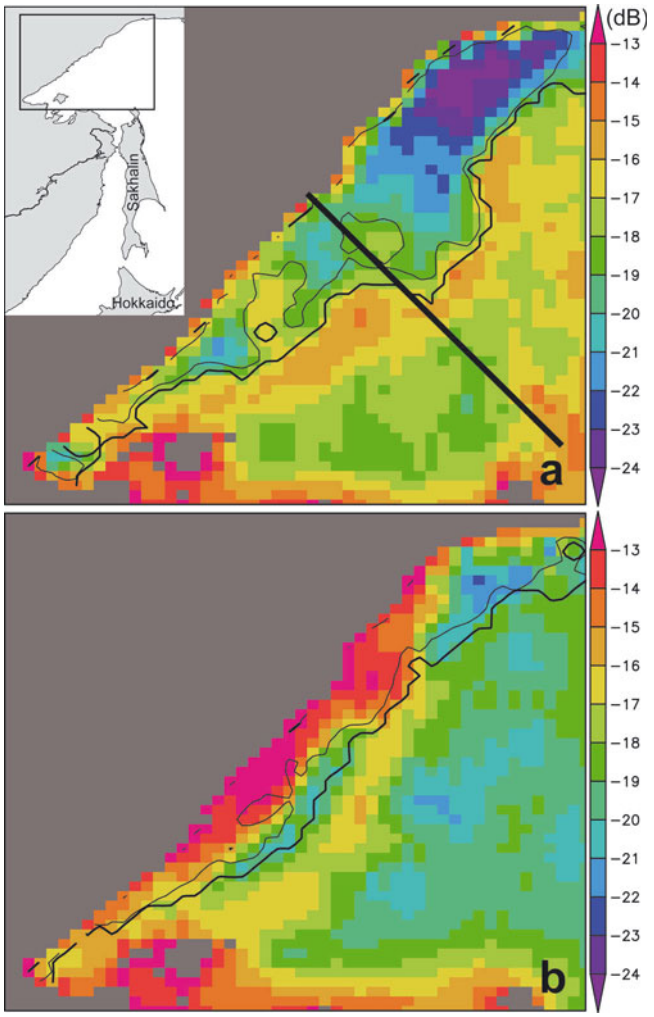

Fig. 3. Maps of horizontally polarized backscatter from the QuikSCAT in the NWS polynya region on (a) 3 February 2003 and (b) 5 March 2003. The backscatter is interpolated onto the AMSR-E grid with a Gaussian weighting function. Thick (thin) contours indicate ice thickness of 0.2 m (0.1 m) from the AMSR-E. The inset in (a) shows the western part of the Sea of Okhotsk wherein a box denotes the enlarged portion. The solid line in (a) indicates the analysis line, L1, shown in Figure 1.

A map of QuikSCAT backscatter in the NWS region on 3 February 2003, when the NWS polynya was well developed, is shown in Figure 3a with isobars of AMSR-E thin-ice thickness superimposed. Most of the coastal polynya area is covered by thin ice with thickness of ≤0.1 m. The thin-ice (≤0.1 m) area corresponds well with the lower-backscatter (<–18 dB) area. The thickness increases sharply near the edge of the coastal polynya, which

https://doi.org/10.3189/172756411795931624 Published online by Cambridge University Press

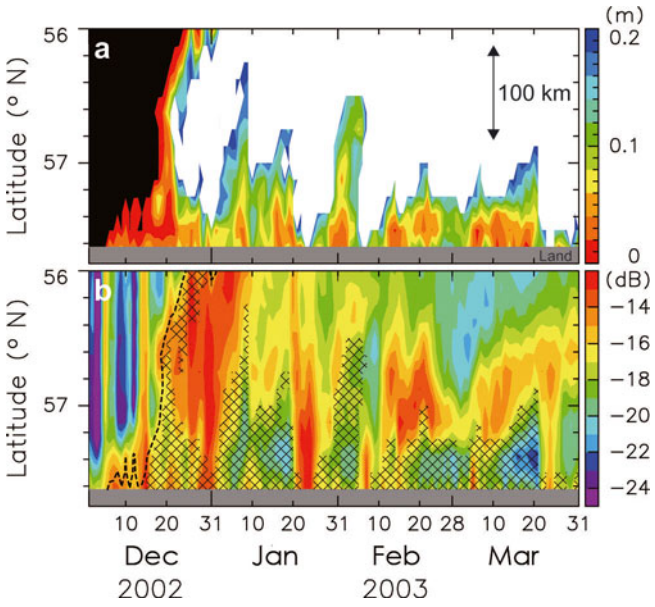

Fig. 4. (a) Daily time series of thin-ice thickness from AMSR-E on the analysis line, L1 (see Fig. 1). The open-ocean (ice concentration <30%) and thicker-ice (>0.2 m) regions are masked by black and white, respectively. (b) Daily time series of horizontally polarized backscatter from QuikSCAT on the analysis line, L1. The dotted line denotes the ice edge. Shadings by cross marks indicate thin-ice (0.2 m) region in (a). The thickness and backscatter data are interpolated every 0.125° of longitude along the line L1.

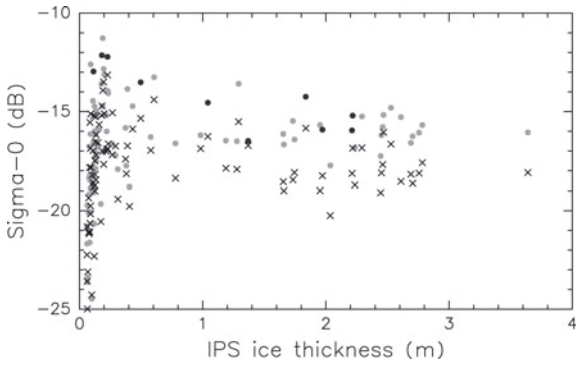

Fig. 5. Scatter plot of the IPS ice thickness versus QuikSCAT backscatter. Crosses and dots denote vertical and horizontal polarization, respectively. The vertically and horizontally polarized backscatters are measured at incidence angles of 54° and 46°, respectively. Black dots indicate windy days in which the geostrophic wind speed exceeds 20 m s^{-1} at an ECMWF gridpoint (52°30′ N, 142°30′ E) closest to the IPS site.

is defined as an ice-thickness contour of 0.2 m. At the outer edge of the polynya, there is a band-like feature with relatively higher backscatter (≥16 dB).

Time series of daily thin-ice thickness and backscatter on the analysis line crossing the NWS polynya (L1 in Figs 1 and 3a) are shown in Figure 4a and b, respectively. In the winter of 2002/03, the sea-ice cover advanced from mid-December. The polynya width is variable, with the maximum width being >100 km from the coast, and the minimum close to 0 km. Most of the coastal polynya area is covered by thin ice with a thickness of ≤0.1 m, and this area corresponds well with the low-backscatter area shown in Figure 3a. The thickness increases sharply near the polynya edge. At the outer polynya edge, a relatively high-backscatter (–16 dB) area exists during most of the polynya period. This corresponds to the band-like feature with relatively higher backscatter in Figure 3a. Data in other years show similar results (not shown here).

The backscatter in the thin-ice (coastal polynya) area occasionally becomes relatively high (>–14 dB; e.g. 5 March 2003 in Fig. 4b). A map of the backscatter and thin-ice thickness in the NWS region on the day is shown in Figure 3b. Contrary to the other cases, the backscatter is high in the thin-ice region where the ice thickness is <0.1 m. In the NWS region, there are only two cases in which the backscatter in the thin-ice (coastal polynya) region is high, as in Figure 3b, during the 5 years 2002/03–2006/07.

3.2. Comparison between QuikSCAT backscatter and IPS ice thickness

In this subsection, the QuikSCAT backscatter is compared with ice draft measured by the IPS in the coastal region of northeastern Sakhalin (black dot in Fig. 1). For the comparison, the IPS ice draft is converted to ice thickness by assuming a water density of 1026.7 kg m^{-3}, ice density of 900 kg m^{-3} and no snow. The no-snow assumption is plausible in thin-ice cases (as in coastal polynyas). Daily mean IPS ice thickness and the backscatter of a pixel closest to the IPS site is used.

Figure 5 is a scatter plot of ice thickness versus backscatter. The backscatter tends to be low when the ice is thin (≤0.1 m). The averaged backscatter of the vertical and horizontal polarization is -20.3 ± 2.8 dB and -19.6 ± 2.8 dB, respectively. The vertically and horizontally polarized backscatter signals show a similar relationship: the backscatter becomes high as ice thickness increases when the thickness is ≤0.2 m, with correlation coefficients of 0.64 for both the vertical and horizontal polarization. The horizontally polarized backscatter seems relatively sensitive to the change in ice thickness. It changes from –24.5 dB to –11.3 dB, while the vertically polarized backscatter changes from –25.0 dB to –13.5 dB when the thickness is ≤0.2 m.

In the case of thicker (>0.2 m) ice, the backscatter is insensitive to the ice thickness (Fig. 5). The averaged backscatter values for ice thickness >0.2 m are -17.4 ± 1.4 dB (vertical polarization) and -15.7 ± 1.4 dB (horizontal polarization).

The backscatter is highest for ice thickness ~0.2 m (Fig. 5). The value is ~–12 dB for the horizontal polarization and is significantly larger than the backscatter of the thicker ice (-15.7 ± 1.4 dB).

3.3. Comparison with photographs of the coastal polynya region near Magadan

Examples of photographs taken from the coast near Magadan (Fig. 1) during winter 2006/07 are shown in Figure 6a–d. During this winter, no pancake ice was observed in this area and all the observed thin ice can be classified as either nilas or grease ice with a smooth surface (Fig. 6a). In many cases, photographically based classification as nilas or grease ice is difficult. From the photographs, three categories, namely 'open water', 'grease ice/nilas' and 'white ice', can be identified. In this study, we define the 'white ice' as whitish ice (e.g. Fig. 6c) which is clearly different from dark thin ice (e.g. Fig. 6a). The 'white ice' is considered to be thicker ice, although it is impossible to estimate ice thickness from the photograph. Subjective

https://doi.org/10.3189/172756411795931624 Published online by Cambridge University Press

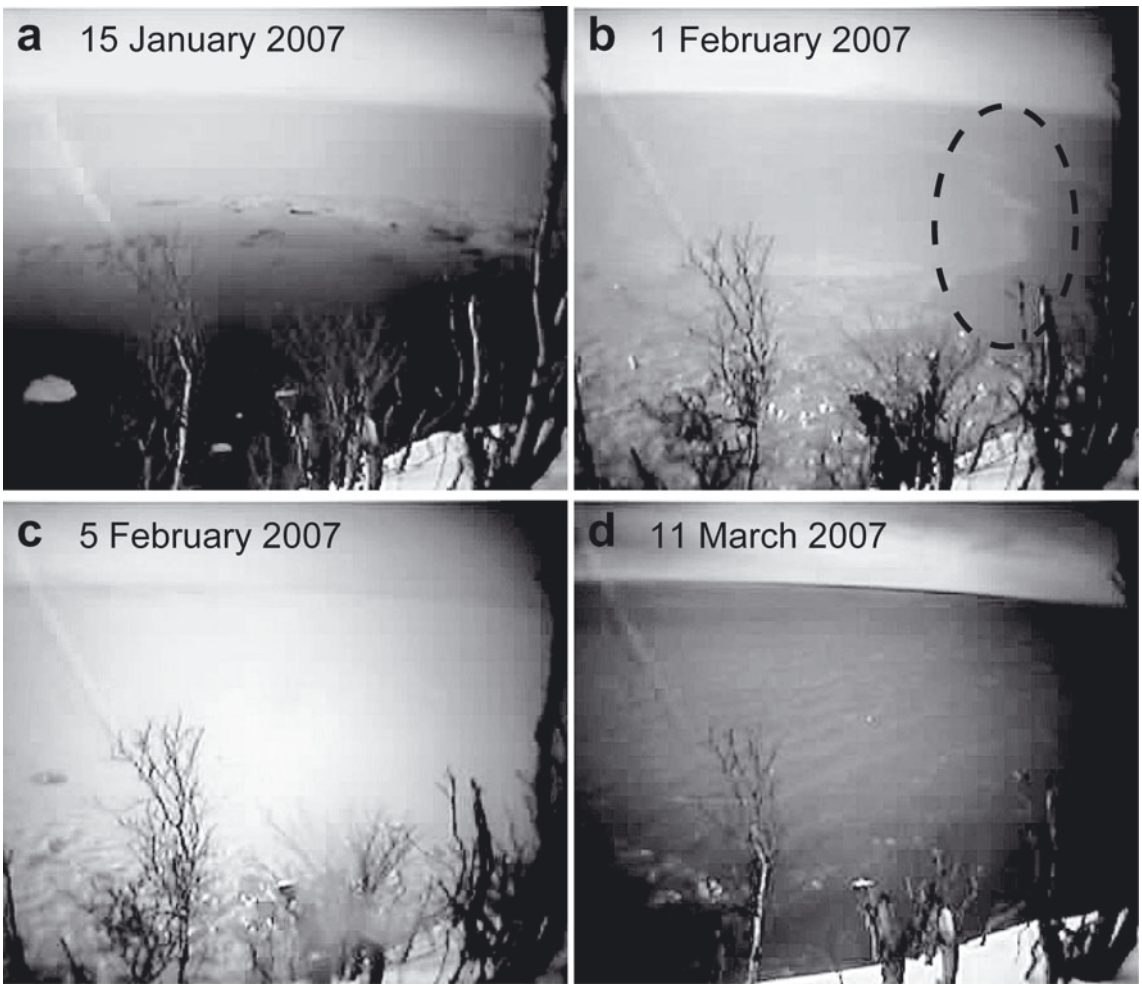

Fig. 6. Photographs of the coastal polynya region taken near Magadan (see Fig. 1) on (a) 15 January 2007, (b) 1 February 2007, (c) 5 February 2007 and (d) 11 March 2007. The photographs also show trees in front of the camera. A white portion at the lower right is land with snow cover. The detail in the circled portion in (b) is described in the text.

classification of the three categories from the daily photographs is shown in Figure 7a.

The photographs show that the coastal region near Magadan had already frozen by 1 December 2006 and was covered with grease ice/nilas. However, AMSR-E ice concentration indicates that the sea ice only existed near the coast until mid-January (Fig. 7b). The photographs show that this region had been covered with thin ice (grease ice/nilas) until 4 February 2007 (Fig. 7a). This is consistent with thin-ice thickness estimated from AMSR-E (Fig. 7c). Daily thin-ice-thickness maps by AMSR-E also show that a coastal polynya formed from late January to 4 February (not shown here). From 1 December 2006 to 24 January 2007, the thin ice within the view range of the camera changed every day. However, for the period 25 January–4 February, a line-like pattern (e.g. circled in Fig. 6b) was seen at almost the same place on the ice surface, and the colour of ice gradually changed whitish. This suggests that the ice motion stopped and the ice thickness increased.

The ice condition changed completely on 5 February 2007, with the colour of ice changing to white and the line-like pattern disappearing (Fig. 6c). This 'white ice' condition continued until 10 March. The AMSR-E ice thickness showed that this region had been covered with thicker ice of thickness >0.2 m during most of the 'white ice' period (Fig. 7a and c). The observation of the ice conditions changing from 'grease ice/nilas' to 'white ice' on 5 February is consistent with the timing of the AMSR-E ice thickness changing from thin ice ($\leq$0.2 m) to thicker ice (Fig. 7a and c).

In photographs after 8 March, open water is shown. At least within the camera range, the coastal region changed to completely open water on 11 March (Fig. 6d). This open-water area is confirmed from ice concentration maps from AMSR-E (not shown here). It is likely that the open-water area was formed by high air temperature (Fig. 7e) caused by the change in wind direction from northwest to southeast (Fig. 7f), associated with the passing of a low-pressure system (not shown here). On 23 March, this region was covered with 'grease ice/nilas' again due to an air-temperature drop associated with the wind direction change. Finally, the ice in this region melted away on 4 April.

The QuikSCAT backscatter at the horizontal polarization averaged for the periods when the ice thickness is estimated as thin ice from AMSR-E (Fig. 7c) is -17.1 ± 1.6 dB (18 January–4 February) and -17.2 ± 1.8 dB (23 March–3 April; Fig. 7d). The backscatter averaged for the thicker-ice period (5 February–7 March) is -15.5 ± 1.9 dB.

4. SUMMARY AND DISCUSSION

This study examined the characteristics of ice in the Okhotsk coastal polynyas using satellite and in situ observed data. In

https://doi.org/10.3189/172756411795931624 Published online by Cambridge University Press

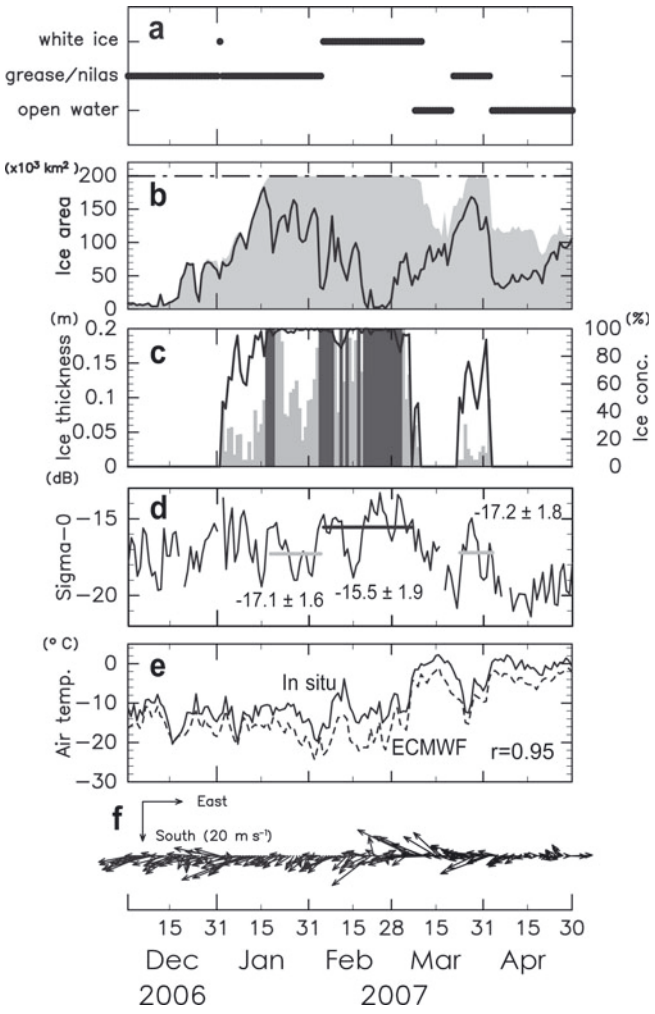

Fig. 7. Time series of daily ice and meteorological conditions in the winter of 2006/07. (a) Ice types subjectively classified from daily photographs taken near Magadan (see Fig. 1). (b) Ice-covered (defined by ice concentration of ≥30%; shading) and thin ice (defined by ice thickness of ≤0.2 m; solid curve) areas in the analysis area, A1 (see Fig. 1). Dash-dotted horizontal line indicates the area of A1. (c) Ice concentration (solid curve) and ice thickness (bars) derived from AMSR-E at a gridpoint shown by a cross in Figure 1. The dark gray bars indicate thicker (>0.2 m) ice. (d) Horizontally polarized backscatter from QuikSCAT at a gridpoint shown by a gray dot in Figure 1. (e) In situ surface air temperature at the camera site, marked by the square in Figure 1 (solid curve) and air temperature at 2 m from ECMWF analysis averaged over four gridpoints, marked by the triangles in Figure 1 (dashed curve). Their correlation coefficient is 0.95. (f) Geostrophic wind vector averaged over the four gridpoints, marked by the triangles in Figure 1. Vertical and horizontal axes correspond to meridional and zonal directions, respectively.

the NWS coastal polynya region, the AMSR-E thin-ice thickness showed that most of the coastal polynya area is covered by thin ice with thickness ≤0.1 m (Figs 3 and 4a). The thickness increases sharply at the edge of the polynya. Comparison with the QuikSCAT Ku-band backscatter showed that the thin-ice (≤0.1 m) area corresponds well with the low-backscatter (≤–18 dB for horizontal polarization at incidence angle of 46°) area almost throughout the coastal polynya period (Figs 3a and 4). The vertically polarized backscatter at incidence angle of 54° showed similar results.

Several factors influence the backscatter of sea ice: surface roughness, salinity (dielectric properties) and the distribution of inhomogeneities such as brine pockets (Tucker and others, 1992). For each ice type, characteristics of the vertically polarized Ku-band backscatter normalized at the 40° incidence angle are summarized as follows (Long and Drinkwater, 1999). Note that the difference of backscatter due to the difference in the incidence angle between 40° and 46° is ~1 dB (Yueh and others, 1997). Volume scattering and surface roughness are the dominant scattering mechanisms in the case of multi-year (perennial) ice. Consequently, backscatter of multi-year ice is high (~–5 dB). For first-year ice, the dominant scattering mechanism is the surface roughness because the salinity is relatively high. As a result, the backscatter is lower at ~–15 dB. The dominant scattering mechanism of thin ice (typically <0.1 m) is also surface roughness.

Thin ice can be roughly classified into three ice types: grease ice, nilas, and pancake ice. The backscatter of grease ice and nilas is considered to be much lower than that of the other ice types, including thick ice, because the ice surface is smooth like a mirror (Tonboe and Toudal, 2005). Long and Drinkwater (1999) showed a value of <–20 dB for nilas. A feature of pancake ice is elevated rims with a nearly uniform height of several centimetres. The rim is formed by collisions between ice floes due to oceanic swells and is considered to act as major roughness elements without directivity (Tonboe and Toudal, 2005). Thus, the result that the thin-ice areas correspond well with the low-backscatter regions (Figs 3a and 4) suggests that the coastal polynyas are covered with grease ice and/or nilas. Occasional cases where the backscatter in the coastal polynya is high (e.g. Fig. 3b) are considered to be caused by pancake ice because these cases are shown simultaneously with windy conditions resulting from the approach of a low-pressure system (not shown). The relatively high-backscatter area at the outer edge of coastal polynyas (Figs 3a and 4) is considered to be caused by the rougher ice surface than the coastal polynya area. This suggests that ice motion in this area may be convergent, and this area may correspond with the collection region of frazil ice in a polynya model proposed by Pease (1987).

Ice thickness measured by an IPS in the coastal polynya region of northeastern Sakhalin (Fig 1) and QuikSCAT backscatter were compared (Fig. 5). The backscatter for both polarizations tends to be low when the ice is thin (≤0.1 m). The averaged backscatter at vertical and horizontal polarizations is –20.3 ± 2.8 dB and –19.6 ± 2.8 dB, respectively. This is consistent with the backscatter for nilas of ~–20 dB (Long and Drinkwater, 1999). The backscatter becomes high as ice thickness increases when the thickness is ≤0.2 m (Fig. 5). The correlation coefficients are 0.64 for both the vertical and horizontal polarizations. The desalination of sea ice during growth is a well-known phenomenon and is due to brine drainage as the ice grows. Hwang and others (2007) showed a negatively correlated relationship between thin-ice thickness and ice surface salinity from in situ observations. The relationship between thin-ice thickness and backscatter (Fig. 5) suggests that the salinity (dielectric properties) possibly influences the backscatter of thin ice.

For thicker (>0.2 m) ice, the backscatter is insensitive to ice thickness and shows similar values (Fig. 5). The averaged backscatter for ice thickness >0.2 m is –17.4 ± 1.4 dB (vertical polarization) and –15.7 ± 1.4 dB (horizontal polarization). This is consistent with the backscatter for

https://doi.org/10.3189/172756411795931624 Published online by Cambridge University Press

first-year ice of ~–15 dB (Long and Drinkwater, 1999). The backscatter for multi-year ice has a higher value of ~–5 dB due to volume scattering associated with the low salinity of the ice caused by brine expulsion and drainage as the ice grows thermally (Long and Drinkwater, 1999). In this study, however, the backscatter of ice with thickness of 0.2 to ~4 m was ~–16 dB (horizontal polarization). This is consistent with the fact that the thick ice in this area has grown up dynamically due to deformation.

The backscatter is highest (~–12 dB for horizontal polarization) for ice thickness ~0.2 m (Fig. 5), suggesting the effect of roughness elements, possibly pancake ice. The cases in which the geostrophic wind speed at an ECMWF gridpoint closest to the IPS site exceeded 20 m s^{-1} are shown by black dots in Figure 5. The backscatter of thin ice tends to be high on windy days, indicating that pancake ice was possibly formed by collisions of new ice owing to oceanic swells caused by the strong wind.

The results from this study were confirmed by photographs taken at the coastal polynya region near Magadan (Fig. 1). During the period when AMSR-E ice thickness was thin (≤0.2 m) and the QuikSCAT backscatter was low (~–17.2 dB for horizontal polarization), the photographs show 'grease ice/nilas' (Figs 6a and 7a, c and d). By contrast, during the period when AMSR-E indicated thick ice (>0.2 m) and the QuikSCAT backscatter was relatively high (~–15.5 dB), the photographs show 'white ice' which is considered to be thicker ice (Figs 6c and 7a, c and d).

In this study, data from in situ ice sampling could not be acquired. In particular, ice salinity, which affects the dielectric properties, is expected to be a key parameter for understanding the relationship between backscatter and thin ice thickness. This will be our future work.

ACKNOWLEDGEMENTS

The QuikSCAT data were obtained from the Physical Oceanography Distributed Active Archive Center (PO.DAAC) at the NASA Jet Propulsion Laboratory. The AMSR-E data were provided by the US National Snow and Ice Data Center (NSIDC), University of Colorado. Comments from the editor and two reviewers were very helpful. This work was supported by Grant-in-Aids for Scientific Research (18201002 and 21740337) from the Ministry of Education, Culture, Sports, Science and Technology (MEXT) of Japan.

REFERENCES

Fukamachi, Y. *and 7 others*. 2009. Direct observations of sea-ice thickness and brine rejection off Sakhalin in the Sea of Okhotsk. *Continental Shelf Res.,* **29**(11–12), 1541–1548.

Hwang, B.J., J.K. Ehn, D.G. Barber, R. Galley and T.C. Grenfell. 2007. Investigations of newly formed sea ice in the Cape Bathurst polynya: 2. Microwave emission. *J. Geophys. Res.,* **112**(C5), C05003. (10.1029/2006JC003703.)

Kitani, K. 1973. An oceanographic study of the Okhotsk Sea: particularly in regard to cold waters. *Bull. Far Seas Fish. Res. Lab.,* **9**, 45–77.

Kwok, R. 2004. Annual cycles of multiyear sea ice coverage of the Arctic Ocean: 1999–2003. *J. Geophys. Res.,* **109**(C11), C11004. (10.1029/2003JC002238.)

Kwok, R. 2007. Near zero replenishment of the Arctic multiyear sea ice cover at the end of 2005 summer. *Geophys. Res. Lett.,* **34**(5), L05501. (10.1029/2006GL028737.)

Long, D.G. 2000. *A QuikScat/SeaWinds sigma-0 browse product, Version 2*. Provo, UT, Brigham Young University.

Long, D.G. and M.R. Drinkwater. 1999. Cryosphere applications of NSCAT data. *IEEE Trans. Geosci. Remote Sens.,* **37**(3), 1671–1684.

Markus, T. and D.J. Cavalieri. 2000. An enhancement of the NASA Team sea ice algorithm. *IEEE Trans. Geosci. Remote Sens.,* **38**(3), 1387–1398.

Martin, S., R. Drucker and K. Yamashita. 1998. The production of ice and dense shelf water in the Okhotsk Sea polynyas. *J. Geophys. Res.,* **102**(C12), 27,771–27,782.

Maykut, G.A. 1978. Energy exchange over young sea ice in the central Arctic. *J. Geophys. Res.,* **83**(C7), 3646–3658.

Nakanowatari, T., K.I. Ohshima and M. Wakatsuchi. 2007. Warming and oxygen decrease of intermediate water in the northwestern North Pacific, originating from the Sea of Okhotsk, 1955–2004. *Geophys. Res. Lett.,* **34**(4), L04602. (10.1029/2006GL028243.)

Nghiem, S.V. *and 6 others*. 2006. Depletion of perennial sea ice in the East Arctic Ocean. *Geophys. Res. Lett.,* **33**(17), L17501. (10.1029/2006GL027198.)

Nghiem, S.V., I.G. Rigor, D.K. Perovich, P. Clemente-Colón, J.W. Weatherly and G. Neumann. 2007. Rapid reduction of Arctic perennial sea ice. *Geophys. Res. Lett.,* **34**(19), L19504. (10.1029/2007GL031138.)

Nihashi, S., K.I. Ohshima, T. Tamura, Y. Fukamachi and S. Saitoh. 2009. Thickness and production of sea ice in the Okhotsk Sea coastal polynyas from AMSR-E. *J. Geophys. Res.,* **114**(C10), C10025. (10.1029/2008JC005222.)

Pease, C.H. 1987. The size of wind-driven coastal polynyas. *J. Geophys. Res.,* **92**(C7), 7049–7059.

Shcherbina, A.Y., L.D. Talley and D.L. Rudnick. 2003. Direct observations of North Pacific ventilation: brine rejection in the Okhotsk Sea. *Science,* **302**(5652), 1952–1955.

Talley, L.D. 1991. An Okhotsk water anomaly: implications for ventilation in the North Pacific. *Deep-Sea Res.,* **38**, Suppl. 1, S171–S190.

Tamura, T., K.I. Ohshima and S. Nihashi. 2008. Mapping of sea ice production for Antarctic coastal polynyas. *Geophys. Res. Lett.,* **35**(7), L07606. (10.1029/2007GL032903.)

Tonboe, R. and L. Toudal. 2005. Classification of new-ice in the Greenland Sea using Satellite SSM/I radiometer and SeaWinds scatterometer data and comparison with ice model. *Remote Sens. Environ.,* **97**(3), 277–287.

Tucker, W.B., III, D.K. Perovich, A.J. Gow, W.F. Weeks and M.R. Drinkwater. 1992. Physical properties of sea ice relevant to remote sensing. *In* Carsey, F.D. *and 7 others, eds. Microwave remote sensing of sea ice*. Washington, DC, American Geophysical Union, 9–28.

Warner, M.J., J.L. Bullister, D.P. Wisegarver, R.H. Gammon and R.F. Weiss. 1996. Basin-wide distributions of chlorofluorocarbons CFC-11 and CFC-12 in the North Pacific: 1985–1989. *J. Geophys. Res.,* **101**(C9), 20,525–20,542.

Yueh, S.H., R. Kwok, S.H. Lou and W.Y. Tsai. 1997. Sea ice identification using dual-polarized Ku-band scatterometer data. *IEEE Trans. Geosci. Remote Sens.,* **35**(3), 560–569.